# Simulation of Ultrasound Backscattering by Red Cell Aggregates: Effect of Shear Rate and Anisotropy

Isabelle Fontaine, David Savéry, and Guy Cloutier
Laboratory of Biomedical Engineering, Clinical Research Institute of Montreal, Montreal, Quebec, H2W 1R7, and Laboratory of Biorheology and Medical Ultrasonics, University of Montreal Hospital, Montreal, Quebec H2L 2W5, Canada

ABSTRACT   Tissue characterization using ultrasound (US) scattering allows extraction of relevant cellular biophysical information noninvasively. Characterization of the level of red blood cell (RBC) aggregation is one of the proposed application. In the current paper, it is hypothesized that the microstructure of the RBCs is a main determinant of the US backscattered power. A simulation model was developed to study the effect of various RBC configurations on the backscattered power. It is an iterative dynamical model that considers the effect of the adhesive and repulsive forces between RBCs, and the effect of the flow. The method is shown to be efficient to model polydispersity in size, shape, and orientation of the aggregates due to the flow, and to relate these variations to the US backscattering properties. Three levels of aggregability at shear rates varying between 0.05 and 10 s$^{-1}$ were modeled at 40% hematocrit. The simulated backscattered power increased with a decrease in the shear rate or an increase in the RBC aggregability. Angular dependence of the backscattered power was observed. It is the first attempt to model the US power backscattered by RBC aggregates polydisperse in size and shape due to the shearing of the flow.

## INTRODUCTION

Ultrasound (US) has become an important imaging modality in the medical field because it is safe, rapid, noninvasive, and relatively inexpensive. The US signal is emitted by a piezoelectric transducer, and, as the mechanical waves propagate through the tissues, a part of the signal is partially scattered back toward the transducer according to the acoustic inhomogeneities encountered. The most well-known application of US backscattering is the formation of B-mode images, obtained by representing the variations in amplitude of the signal backscattered from tissues as gray levels. In recent years, other applications have emerged, such as tissue characterization. Because the properties of the scattered wave vary with size, the acoustic impedance (density and compressibility), and the microstructural organization of the cells, US scattering can be used to detect the presence of tissue abnormalities, such as cancerous cells (Landini and Verrazzani, 1990; Ursea et al., 1998).

For a region of interest in a blood vessel, the main scatterers of the US waves are the red blood cells (RBCs). The backscattered signal is thus associated to the properties of the blood sample, e.g., the hematocrit and the level of aggregation. Red cell aggregation results from complex cellular interactions that depend on the size and concentration of certain proteins in the plasma, the intrinsic deformability of the red cells, their glycocalyx (external layer), and the hematocrit. The aggregative tendency of RBCs changes among individuals and is modulated by the flow conditions, which vary within the arterial/venous tree. Thrombosis (Chabanel et al., 1994), hypertension (Razavian et al., 1992), hyperlipidemia (Razavian et al., 1994), diabetes (Schmid-Schönbein and Volger, 1976), and coronary artery disease (Neumann et al., 1991) are, among others, pathologies often associated with abnormally high levels of RBC aggregation. It would therefore be valuable to detect such abnormalities by US methods, but the relation between the level of aggregation and the US measurements is still unclear.

Experimental measurements have shown that the US backscattered power increases with the level of RBC aggregation (Cloutier and Qin, 1997). It was observed that the US power backscattered by aggregating RBCs, such as human, porcine, or equine RBCs, was shear-rate-dependent (Sigel et al., 1982; Yuan and Shung, 1988; Shehada et al., 1994; Cloutier and Qin, 2000), whereas the US power backscattered by nonaggregating RBCs, such as bovine RBCs or a saline suspension of RBCs, was little affected by the shearing condition (Yuan and Shung, 1988). In the studies performed with aggregating RBCs, power variations of the order of 15 dB were observed as a function of the shear rate at acoustical frequencies below 10 MHz. Moreover, it was observed that the dependence of the backscattered power with the frequency of insonification is modified by the level of aggregation (Foster et al., 1994). There is thus a need to provide a model of US backscattering by aggregating RBCs to interpret these experimental findings and shed some light on the mechanisms of US backscattering by blood.

Many models were proposed to characterize US backscattering, however the majority of them addressed the problem of nonaggregating RBCs (Berger et al., 1991; Mo and Cobbold, 1992; Zhang et al., 1994). Our group recently simulated US backscattering by RBCs by modeling the US system characteristics and the RBCs' shape and positions

---

(Fontaine et al., 1999; Teh and Cloutier, 2000). These models guided us to formulate the following hypothesis: the spatial organization of aggregating RBCs is the main determinant of the US backscattered power. Several authors studied the ultrasonic signal signature as a function of the spatial organization of scatterers (Landini and Verrazzani, 1990; Varghese and Donohue, 1993). Unfortunately, their modeling approaches could hardly be applied to a complex medium such as blood, because they modeled regularly positioned scatterers, isotropic media, or dilute systems of scatterers. To our knowledge, the positions of aggregated RBCs cannot easily be related to a known spatial distribution. Furthermore, the eventual presence of spatial anisotropy in the medium adds more complexity to the modeling.

The purpose of this study is to determine the effect of realistic configurations of RBCs, and to study whether a change in their spatial organization would lead to significant variations of the US backscattered power. To achieve this, an iterative flow-dependent simulation model of aggregating particles was developed. To solely study the effect of the positioning of the particles, the suspension of RBCs was modeled by spheres. A wide variety of configurations of RBCs was obtained by varying both the flow shear rate, and the strength of interactions between the red cells. Modeling the exact mechanisms of RBC aggregation is outside the scope of this paper. To our knowledge, it is the first attempt to model polydispersity in size, shape, and orientation of aggregates due to the shearing of the flow and to relate these variations to US backscattering.

The next section presents a brief overview of the theoretical principles underlying the mechanisms of RBC aggregation and US backscattering by blood. This section is followed by the description of the dynamic model of RBC aggregation, which includes the effect of the flow as well as the repulsive and adhesive forces modeled according to the intrinsic aggregability of RBCs. Then, the model used to estimate the backscattered US signal and the backscattered power is described. The results and discussion are presented next. In conclusion, the proposed dynamic aggregation modeling approach is shown to be an efficient tool to simulate realistic structural arrangements of RBCs under shear flow. The structure factor of the aggregates is proposed to relate the backscattered power to the microstructural properties of RBCs. The simulation results are compared to experimentally measured variations of the US backscattered power with the angle of insonification (Allard et al., 1996).

## THEORY

### Mechanisms of RBC aggregation

Two mechanisms were proposed to explain the aggregation of RBCs, the bridging model and the depletion model. According to the bridging model, the formation of RBC aggregates results from the adsorption of plasmatic macromolecules at the surface of the RBCs (Chien, 1975; Brooks et al., 1980; Chien, 1981). In contrast, the depletion model suggests that the exclusion of the plasmatic macromolecules near the surface of RBCs induces aggregation (Bäumler et al., 1996; Armstrong et al., 1999). The depletion layer would result in a reduction of the osmotic pressure in the gap between two nearby RBCs, creating an attractive force between them. In addition to the adhesive forces, due to either adsorption or depletion of macromolecules and the Van der Waals forces, which are always present in a colloidal suspension, there are repulsive forces that hinder the formation of RBC aggregates. The main repulsive forces are the steric forces due to the glycocalyx, and the electrostatic repulsive forces due to the presence of negative charges at the surface of RBCs (Bäumler et al., 1989). The flow also plays a significant role in the phenomenon of RBC aggregation. At low shear rates, the flow can promote RBC aggregation, whereas, at higher shear rates it rather has a dispersing effect.

### Mechanisms of US backscattering by blood

US backscattering by blood is a complex phenomenon to characterize because of the high density of RBCs in blood. Tissue scattering properties are often described by their backscattering coefficient (BSC) that is, by definition, the average power backscattered per steradian by a unit volume of blood, insonified by a monochromatic plane wave of unit intensity (Shung and Thieme, 1993). For a suspension of weak identical scatterers (weak in the sense that the acoustic impedance of the scatterers is similar to that of the suspending plasmatic medium), it is given by

$$\text{BSC} = \sigma_{\text{bs}}(H/V)S, \tag{1}$$

where $\sigma_{\text{bs}}$ is the backscattering cross-section of a single scatterer (i.e., the power backscattered by a single particle), $H$ is the hematocrit, $V$ is the volume of the identical scatterers, and $S$ is the structure factor. Both $\sigma_{\text{bs}}$ and $S$ depend on the incident acoustic wave frequency. Similar forms of the previous equation can be found in the literature (Mo and Cobbold, 1992; Twersky, 1987). For Rayleigh scattering, which implies that the wavelength of the incident wave is much larger than the size of the scatterers, the backscattering cross-section ($\sigma_{\text{bs}}$) is proportional to the square of the particle volume and to the fourth power of the incident wave frequency (Shung and Thieme, 1993; Fontaine et al., 1999). The structure factor ($S$) characterizes the spatial organization of the scatterers in the frequency domain. The frequency domain highlights the periodicities in the tissue microstructure, emphasizing the most recurrent interparticle intervals. In crystallography and other fields of research, the structure factor is often computed by x-ray diffraction to

characterize the microstructure of small molecules. For US backscattering, it is equal to (Twersky, 1975)

$$S(\mathbf{k}) = 1 + \rho \int e^{-j2\mathbf{kr}}[g(\mathbf{r}) - 1]\, d\mathbf{r}, \qquad (2)$$

where $\mathbf{k}$ is the wavevector ($\mathbf{k} = 2\pi\, \mathbf{e}_{inc}/\lambda$, where $\mathbf{e}_{inc}$ is the unit vector showing the direction of the incident wave, and $\lambda$ is the wavelength), $\rho$ is the number density of the particles, and $g(\mathbf{r})$ is the pair-correlation function that represents the normalized probability of finding two particles separated by a distance $\mathbf{r}$. In other words,

$$g(\mathbf{r}) = \frac{\mathrm{P}(\mathbf{x}\ \text{and}\ \mathbf{x} + \mathbf{r}\ \text{are particle centers})}{\mathrm{P}(\mathbf{x}\ \text{is a particle center})^2}, \qquad (3)$$

where P indicates the probability. As the positions of the particles become uncorrelated, the pair-correlation function tends toward 1. The distance of correlation refers to the largest distance $\mathbf{r}$ such that $g(\mathbf{r}) \neq 1$.

If the positions of the particles are correlated only on short distances in comparison to the wavelength, the BSC (Eq. 1) can be estimated by using the low-frequency limit of the structure factor, called the packing factor ($W$). From Eq. 2,

$$S(\mathbf{k} \to 0) \approx W = 1 + \rho \int [g(\mathbf{r}) - 1]\, d\mathbf{r}. \qquad (4)$$

The packing factor of totally uncorrelated particles in space is equal to 1, whereas it takes the value of 0 for perfectly ordered particles (crystallographic arrangement). In the case of identical nonaggregating hard spheres, the packing factor is entirely determined by the number density of particles, and it can be estimated by using the Percus–Yevick approximation (Twersky, 1975). The packing factor ($W$) can be shown to be the ratio of the variance of the number of particles per voxel to the mean number of particles per voxel, when it is large compared to the size of the aggregates. This approximation was used in the modeling of the US backscattered power by nonaggregating RBCs at low frequencies (Lucas and Twersky, 1987; Mo and Cobbold, 1992; Lim et al., 1996; Fontaine et al., 1999). In this particular case, backscattering at low frequencies is independent of the incident wave orientation because the packing factor is not angular dependent.

It is still unclear if the packing factor approximation is fully valid in the presence of RBC aggregates because the distance of correlation between the positions of the particles can increase significantly in this case. Moreover, because an angular dependence of the backscattered power for aggregating RBCs was observed at 10 MHz (Allard et al., 1996), this suggests that the length of correlation of aggregated RBCs may be too important to ensure the validity of the low-frequency approximation (Eq. 4) at this frequency.

Thus, the anisotropy of the pair-correlation function $g(\mathbf{r})$ should be taken into consideration for modeling US backscattering by aggregated RBCs.

Alternatively to Eq. 2, the structure factor can also be expressed as a function of the microscopic density $N$, defined by the center position of each particle $\mathbf{r}_i = (x_i, y_i)$. This function is defined two dimensionally by

$$N(x, y) = \sum_{i=1}^{M} \delta(x - x_i, y - y_i), \qquad (5)$$

and

$$S(\mathbf{k}) = \frac{1}{M} \left| \mathscr{F}(N) \right|^2 = \frac{1}{M} \left| \sum_i e^{-j2\mathbf{k} \cdot \mathbf{r}_i} \right|^2, \qquad (6)$$

where $M$ is the number of scatterers, $\delta$ is the Dirac function, and $\mathscr{F}(N)$ is the Fourier transform of the microscopic density function.

The power spectrum of the microscopic density function of a suspension of perfectly random scatterers is constant over the whole range of frequencies (Poisson point process). Because the position that a particle can take is constrained by the presence of its neighbors, the positions of a large number of nonoverlapping (rigid) particles cannot be totally random in a given volume. Thus, the structure factor of such a suspension is characterized, in the spectral domain, by regular oscillations, whose period can be related to the size of the particles. In the case of nonaggregating RBCs at a hematocrit of 40%, the oscillation frequency is >100 MHz (Fontaine et al., 1999). Because RBC aggregation results in an increase of the correlation length, the amplitude of the oscillations of $S(\mathbf{k})$, and its low-frequency limit should be different from the case of no aggregation. In the present study, in addition to the structure factor given by Eq. 6, the pair-correlation function $g(\mathbf{r})$ was also determined to understand the effect of RBC aggregation on the length of correlation. From Eqs. 2 and 6, it can be shown that the pair-correlation function $g(\mathbf{r})$ is obtained from the inverse Fourier transform of the structure factor.

## METHODS

### Aggregation modeling

An iterative two-dimensional (2D) model was developed to simulate the formation of RBC aggregates in a Couette shear flow. The proposed 2D dynamic model takes into consideration the displacement due to the adhesive and repulsive forces between RBCs and the effect of the flow. The interaction between pairs of particles was modeled according to their intercellular distance. The exact mathematical expressions describing the interactions between RBCs are not known, because the mechanisms of RBC aggregation still remain ambiguous (depletion or adsorption), and because these interactions fluctuate significantly according to the type and concentration of macromolecules in the plasma. Nevertheless, it can be assumed that the adhesion between two red cells will occur only if those particles are close enough. Moreover, the adhesive forces have to be greater than the forces that tend to disaggregate the particles, i.e., the electrostatic and steric forces, and the effect of the flow. Thus, the level of

aggregation results from multiple forces that depend on the positions of the red cells in the medium, with respect to the surrounding particles. In the current model, the motion of the RBCs was defined according to the summation of the displacement resulting from each type of force (attraction, repulsion, and flow shear motion). The model includes the possibility to consider RBC hyperaggregation by modifying the importance of the adhesive forces with respect to the other forces.

The particles were initially positioned randomly without overlap in a 2D space of 300 by 300 $\mu$m. The simulated hematocrit was 40% (corresponding to ~1500 particles in the region of interest, ROI), each RBC being modeled by a disk of 5.5 $\mu$m in diameter. This diameter was selected to match an average volume of RBCs of 87 $\mu$m$^3$. At each time step, the vector displacements resulting from each force were summed for every RBC. Once the displacements were computed for all particles, they were moved for the next iteration. The process was continued until the size of the aggregates reached a steady state. Simulations of RBC aggregation were performed at shear rates of 0.05, 0.08, 0.1, 0.3, 0.5, 1, 2, 5, 8, and 10 s$^{-1}$. Three levels of RBC aggregability were modeled.

The accuracy of such an iterative dynamical model is limited by the sampling of the time scale and the finite spatial window. Even if new developments would allow for modeling more accurately the adhesive/repulsive forces (Donath and Voigt, 1986), it would be difficult to implement the aggregation process numerically with such precision. A single simulation already required several days to reach the stable state. As explained below, the choice of the quantitative parameters of the model was mainly performed to obtain different levels of aggregation and to minimize particle superposition. The parameters were also selected to allow the rotation of the aggregates at low shear rates, as opposed to disaggregation at high shear rates. Even with those limitations imposed by the numerical modeling strategy (disks, 2D model, finite spatial window, time sampling), the results are innovative, because they allow the understanding of the effect of specific organizational characteristics of RBCs and RBC aggregates, modulated by the shear rate, on the US backscattered power.

### Displacement related to the flow

The displacement of one particle due to the flow depends on its position in the ROI because a predetermined velocity profile was imposed. For a Couette flow, which can be obtained in the gap between two coaxial cylinders, the velocity component of a point particle is proportional to the shear rate and its radial coordinate. According to the reference axes schematized in Fig. 1 *a*, the radial position of the particle (axis *y*) determines its velocity along the *x* axis. The motion of one RBC along *x* was described by

$$(v_x)_{flow} = \gamma y \quad \text{and} \quad (\Delta x)_{flow} = (v_x)_{flow} \Delta t, \qquad (7)$$

where $(v_x)_{flow}$ represents the fluid velocity along *x*, $\gamma$ is the shear rate, and *y* is the radial position perpendicular to the cylinders. The variable $\Delta x$ is the displacement of the RBC within a discrete time increment $\Delta t$. The radial velocity $(v_y)_{flow}$ was supposed null (no secondary flow). Figure 1 *b* illustrates the magnified ROI and the velocity profile of the RBCs. When a RBC was moved outside the ROI ($x = 300 \ \mu$m + $\xi$), the RBC was reentered in the ROI at $x = \xi$. The chosen time increment could not be too small to limit the time required to run the simulations. In contrast, a large time increment did not allow enough precision in the motion of the RBCs. A time increment $\Delta t = 10$ ms appeared to be a good compromise.

### Displacement related to the adhesive and repulsive forces

The formation of RBC aggregates requires the presence of macromolecules in the plasma. The intercellular distance between aggregated RBCs is a function of the length of the bond (bridging model), or of the thickness of the depletion layer (depletion model). Fibrinogen is the primary macro-
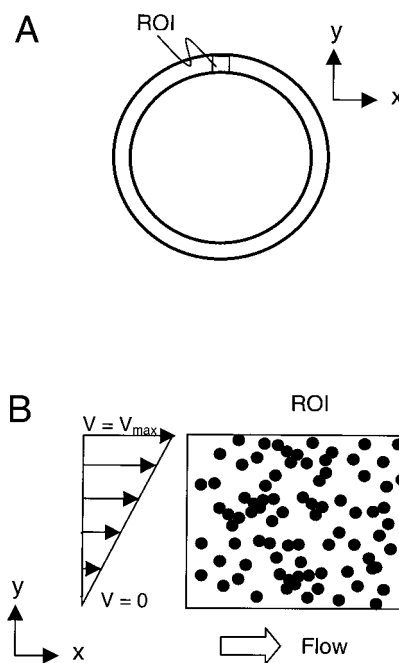


FIGURE 1 (*A*) Top view of the two coaxial cylinders composing the Couette flow system. The ROI is located in the small gap between the two cylinders. The *x* axis refers to the direction of the flow parallel to the cylinders, and the *y* axis refers to the radial direction between the cylinders. (*B*) Magnification of the ROI and illustration of the velocity profile, assuming a constant shear rate in the ROI.

molecule in normal plasma that causes RBC aggregation. Previous studies (Jan and Chien, 1972; Chien, 1981) estimated the intercellular distance between aggregated RBCs in the presence of fibrinogen to 25 nm by electron microscopy. Although this technique is subjected to artifacts due to the preparation of the cells (RBCs are sedimented, fixed, and dehydrated) and due to the intrinsic limitations of the measurement method, this distance represents enough precision for the current model. Thus, this value was taken as a reference to model the equilibrium distance of a doublet of RBCs.

### Displacement related to the repulsive forces

The displacement resulting from the repulsive forces was modeled as illustrated in Fig. 2. It was assumed constant for intercellular distances (*d*) smaller than 25 nm (center–center distance varying between 0 and 5.525 $\mu$m). Because of the finite time resolution, the particles could temporarily be brought closer to each other than the equilibrium distance of 25 nm. When this happened, the repulsive forces, that include the steric and the electrostatic effect, were modeled to put back the RBCs at distances larger than 25 nm. According to Fig. 2, when two RBCs were separated by <25 nm, they were moved by 12.5 nm in the opposite direction (the angle of the doublet in the 2D space was maintained when moving the cells). This displacement corresponds to half the equilibrium intercellular distance (25 nm/2). For intercellular distances >25 nm, the repulsive force was modeled as an exponentially decreasing function. The rate of decrease of the repulsive force was set equal to the Debye–Hückel constant, $\kappa$, which is equal to the reciprocal of the double layer thickness (0.8 nm)$^{-1}$ for normal red cells in a saline solution (0.9% NaCl) (Chien, 1981; Jan and Chien, 1973). The repulsive forces were only considered for intercellular distances <50 nm because of the very fast decay of the exponential function. In
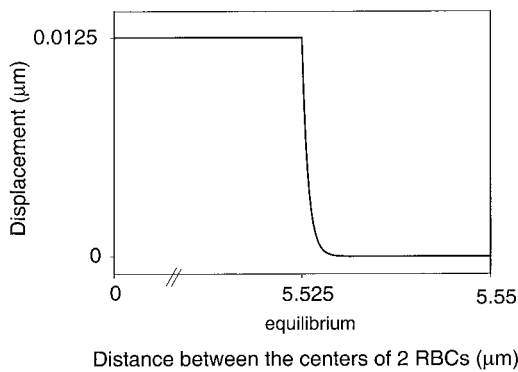
FIGURE 2   Displacement resulting from the repulsive forces expressed as a function of the distance separating two neighboring RBCs (center–center).

summary, the motion due to the repulsive forces resulting from the presence of two RBCs centered at $\mathbf{r}_i$ and $\mathbf{r}_j$ can be written as

$$|\Delta\mathbf{r}|_{repul} = 12.5 \text{ nm}$$

$$\text{if} \quad 0 \le |\mathbf{r}_i - \mathbf{r}_j| \le 5.525 \ \mu m \tag{8a}$$

$$|\Delta\mathbf{r}|_{repul} = 12.5e^{-\kappa(d-0.025)} \text{ nm}$$

$$\text{if} \quad 5.525 \ \mu m < |\mathbf{r}_i - \mathbf{r}_j| \le 5.55 \ \mu m \tag{8b}$$

$$|\Delta\mathbf{r}|_{repul} = 0$$

$$\text{otherwise,} \tag{8c}$$

where $\kappa = 1.25 \times 10^3 \ \mu m^{-1}$, and the intercellular distance $d = |\mathbf{r}_i - \mathbf{r}_j| - 5.5 \ \mu m$.

### Displacement related to the adhesive forces

According to several authors, the aggregation level of normal RBCs is stable or increases as the shear rate is raised from 0 to ~0.5 s$^{-1}$ (Chien, 1976; Copley et al., 1976). This a priori information was used for the modeling of the displacement attributed to the adhesive forces (adsorption

or depletion forces). The effect of the adhesive forces was determined to avoid disaggregation of an existing doublet positioned perpendicular to the Couette flow direction at 0.5 s$^{-1}$. The adhesive displacement necessary to maintain the doublet aggregated was set to 40.5 nm in the direction of the other RBC, for RBCs separated by less than 50 nm (this distance is arbitrarily selected to twice the postulated equilibrium RBC intercellular distance to consider the discrete nature of the model). The adhesive displacement was set to 40.5 nm for intercellular distances between 0 and 50 nm (center–center distances varying between 5.5 and 5.55 $\mu m$), whatever the angle of the doublets. When cellular overlap occurred at a given iteration (center–center distances <5.5 $\mu m$), the adhesive forces were supposed to be null. No displacement due to the adhesive forces was considered for intercellular distances larger than 50 nm.

### Modeling of hyperaggregation

Hyperaggregation was modeled by modifying the amplitude of the displacement related to the adhesive forces, or its domain of influence. Two levels of hyperaggregation were considered. The intermediate level was obtained by considering the adhesive and repulsive forces for RBCs separated by <75 nm (instead of 50 nm for the case of the lowest aggregability). The same displacement as in the original modeling was then applied for the adhesive forces (40.5 nm). The highest RBC aggregability was obtained by considering the adhesive forces for RBCs separated by <100 nm. The displacement resulting from the application of the adhesive forces was also more important, i.e., 60 nm instead of 40.5 nm for the lowest and the intermediate levels of RBC aggregability.

At each iteration, the displacements resulting from the adhesive and repulsive forces, and from the flow were summed as schematized in Fig. 3. The displacement related to the flow is always parallel to the x axis, and the direction of the displacement related to the adhesive and repulsive forces depends on the position of the neighboring particles. For clarity, the latter was only illustrated for one of the two particles composing the doublet. The net displacement was computed by a vectorial summation, and all the RBCs were moved at the same time. Note that the magnitudes of the displacements in Fig. 3 are not illustrated at the real scale, to facilitate the reading. The combined effect of all forces on a single rouleau of five RBCs can be observed in Fig. 4. At a low shear rate of 0.1 s$^{-1}$, the rouleau tended to rotate and to be aligned with the flow after several iterations. At 0.5 s$^{-1}$, the 5-cell aggregate was disrupted to the size of a doublet. The doublet also rotated with the flow. At a high shear, the rouleau was broken into individual cells. This simple behavior, presented here to illustrate the modeling process, becomes more complex when the aggregate is surrounded by numerous cells/aggregates, at a normal hematocrit.
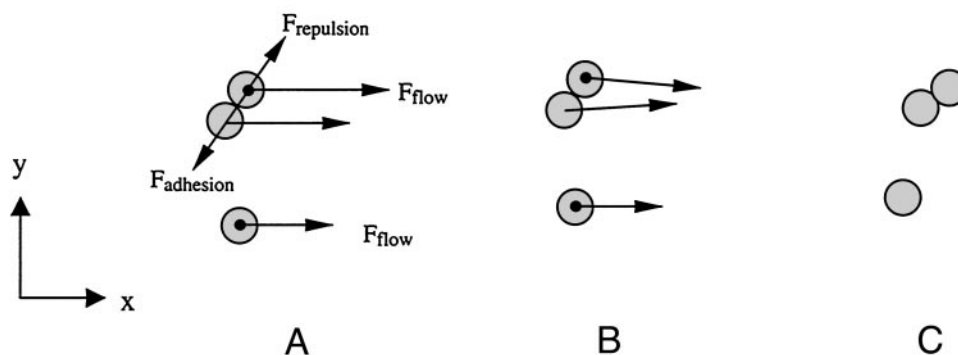


FIGURE 3   An example of the vector displacements considered in the dynamic simulation of RBC aggregation. (a) Illustration of the vector displacement resulting from each force. The displacement resulting from the flow is parallel to x, and is proportional to the radial position of the RBC (y). The adhesive force is directed toward the RBC that causes the force, and the repulsive force is oriented in the opposite direction. For clarity, they were illustrated only for one of the two RBCs composing the doublet (they are the exact opposite for the other RBC). (b) Resulting vector displacement after summation. (c) Configuration of the RBCs after motion from one iteration.
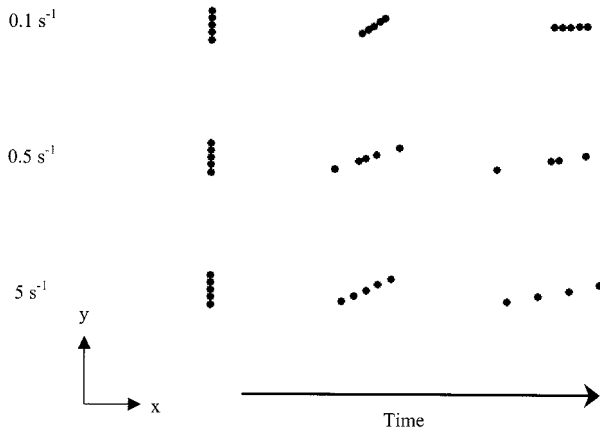
FIGURE 4   Motion of a single rouleau of five RBCs resulting from the combined effect of all simulated forces for different iterations (time increments). The examples correspond to the lowest aggregability simulated at shear rates of 0.1, 0.5, and 5 s$^{-1}$.

## Ultrasound backscattering modeling

The simulation model of the US backscattered radio-frequency (RF) signal is described in details elsewhere (Fontaine et al., 1999). The simulation model assumes a linear mode of propagation of the acoustic waves in a weak scattering medium (Born approximation), and is valid for a small region of interest in the far field of the transducer. The backscattered RF signal can then be modeled as the convolution of the US system characteristic function (T), the function characterizing the acoustical impedance mismatch of the RBC with respect to the surrounding media (C), and the microscopic density function (N). In two dimensions,

$$RF(x, y) = \frac{\partial^2}{\partial y^2} T(x, y) \otimes C(x, y) \otimes N(x, y), \quad (9)$$

where $y$ is the ultrasonic wave direction of propagation corresponding to the direction perpendicular to the flow motion (Fig. 1).

The transducer transfer function was modeled as a Gaussian envelope modulated by a cosine function,

$$T(x, y) = \exp\left[\frac{-1}{2}\left(\frac{x^2}{\psi_x^2} + \frac{y^2}{\psi_y^2}\right)\right]\cos\left(\frac{4\pi f y}{c}\right). \quad (10)$$

In the above equation, $\psi_x$ and $\psi_y$ are the standard deviations of the 2D Gaussian function representing the beamwidth and the bandwidth of the transmitted waves. The beamwidth defines the lateral resolution of the measuring system, whereas the bandwidth determines the axial resolution (a large bandwidth corresponds to a good axial resolution, and vice-versa). The parameter $2f/c$ in Eq. 10 represents the transducer spatial frequency, where $f$ is the ultrasonic frequency and $c$ is the speed of sound. In the current manuscript, the US system was modeled with $\psi_x = 0.43$ mm, $\psi_y = 0.03$ mm, and $f = 10$ MHz. The selected value of $\psi_y$ corresponds to a bandwidth of ~10 MHz at −3 dB (wideband signal). The speed of US, $c$, in blood was assumed equal to 1570 m/s. In theory, the BSC given by Eq. 1 corresponds to the insonification of the medium by a monochromatic plane wave (infinitely small bandwidth). In the current simulation, a 10-MHz bandwidth was modeled, which better represents realistic transducer responses for backscattering experiments.

The convolution operation (Eq. 9) implies that all RBCs are identical in shape and impedance. The function C, describing the shape and the

mismatch in acoustic impedance of each RBC, was modeled as the projection of a sphere. In 2D,

$$C(x, y) = 2\sqrt{a^2 - x^2 - y^2} \quad \text{for} \quad x^2 + y^2 \leq a^2, \quad (11)$$

where $a = 2.75$ $\mu$m represents the radius of the simulated spherical RBC.

The 2D aggregation model described earlier was used to generate the function N. This function characterizes the position of each RBC in the 2D space. It was computed from the $x$ and $y$ coordinates of the center of all RBCs. Each simulation, performed from different random initial spatial conditions, was repeated four times to allow statistical averaging. All simulations were performed with MATLAB 5.3 (The MathWorks Inc., Natick, MA).

### Rotation of the transducer

To allow the study of the anisotropy of the backscattered power, US backscattering was modeled at various angles of insonification by doing a rotation of the transducer transfer function. As performed by Teh and Cloutier (2000), the $x$–$y$ plane in Fig. 1 was mapped onto the $p$–$q$ plane. The function characterizing the transducer was computed on the rotated axes. The following equations were used to transform the $x$–$y$ plane onto the $p$–$q$ plane:

$$\begin{bmatrix} p \\ q \end{bmatrix} = \begin{pmatrix} \sin\theta & \cos\theta \\ -\cos\theta & \sin\theta \end{pmatrix} \begin{bmatrix} x \\ y \end{bmatrix}, \quad (12)$$

where $\theta$ represents the angle of rotation of the axes. Thus, 0° corresponds to a direction of insonification parallel to the flow, whereas 90° represents a direction perpendicular to the flow direction.



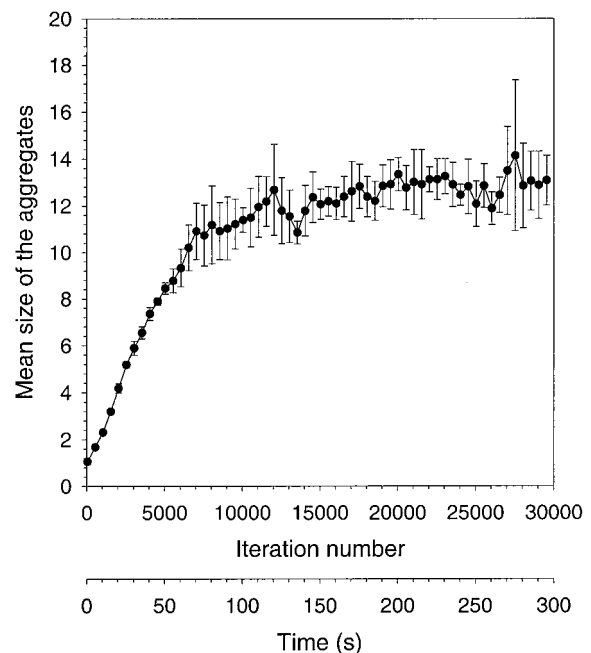FIGURE 5   Mean size of the aggregates (mean number of RBCs/aggregate) as a function of the number of iterations (time) of the simulation model, at 0.1 s$^{-1}$, for the lowest RBC aggregability. Results are expressed in terms of mean ± one standard deviation ($n = 4$). A mean aggregate size of 1 corresponds to a single RBC.
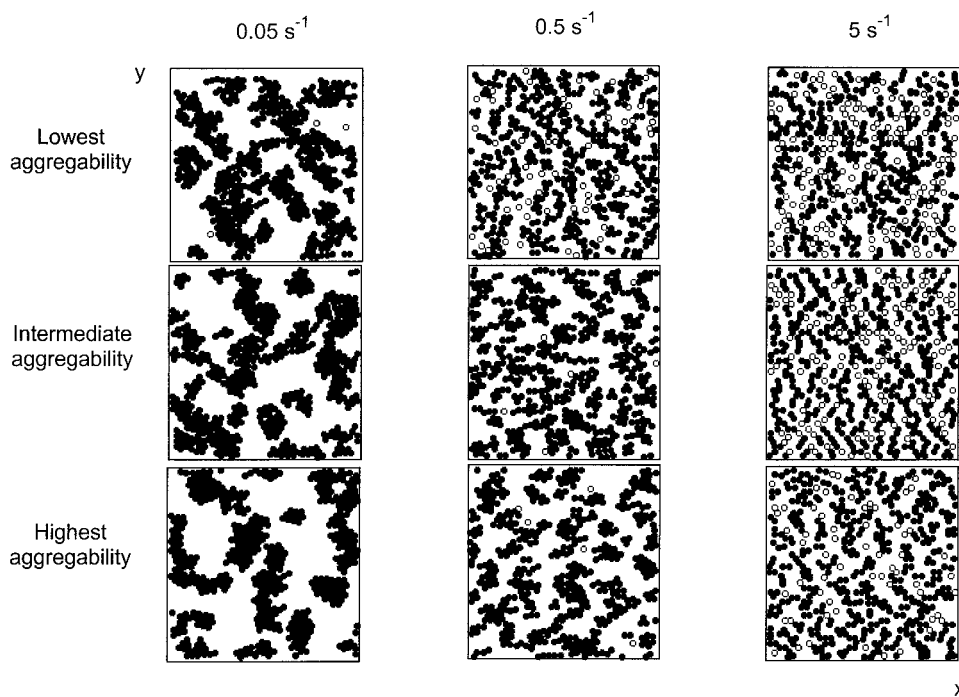
FIGURE 6 Simulation results of RBC aggregation at 40% hematocrit. Filled circles represent aggregated RBCs, and empty circles represent nonaggregated cells. Zoomed areas of 180 by 180 $\mu$m are illustrated. The simulated areas are 300 by 300 $\mu$m. Each panel was obtained at the steady state of aggregation (plateau of the kinetics of aggregation, see Fig. 5).

### Computation of the US backscattered power

The backscattered power was computed on the 2D spectrum of the RF image obtained from Eq. 9. The spectrum of the RF image was computed from the central portion (256 by 256 $\mu$m) of the simulated ROI to avoid errors from the edges. The backscattered power (POW) was computed from the spectrum of the transducer transfer function (T) previously derived, the spectrum of the cell function (C) and that of the microscopic density function (N),

$$\text{POW} = \frac{1}{M_s} \sum_{f_x} \sum_{f_y} \left| \mathscr{F}\left(\frac{\partial^2}{\partial y^2} \text{T}\right) \mathscr{F}(\text{C}) \mathscr{F}(\text{N}) \right|^2, \quad (13)$$

where $M_s$ is the number of samples in the frequency domain ($f_x, f_y$).

## RESULTS

### Aggregation modeling

Figure 5 shows the evolution of the mean size of the aggregates as a function of the iteration number (time), for a shear rate of 0.1 s$^{-1}$ and the lowest aggregability ($n = 4$). The application of a constant shear rate resulted in an increase of the mean size of the aggregates as a function of time. The number of iterations required to reach the steady state and the maximum size of the aggregates varied with the shear rate and the RBC aggregability.

Figure 6 shows different structures of RBC aggregates obtained with the simulation model for different shear rates and RBC aggregabilities. Filled circles represent aggregated

RBCs, and empty circles represent nonaggregated cells. The number of aggregated RBCs and the size of the aggregates increased as the shear rate was decreased or the aggregability was raised. Figure 7 illustrates the mean size of the aggregates obtained at the steady state of aggregation (plateau in Fig. 5) for all simulated conditions. At the lowest shear rate of 0.05 s$^{-1}$, the mean number of RBCs per aggregate was 24.9 $\pm$ 1.8, 39.6 $\pm$ 3.6, and 45.8 $\pm$ 4.1 for the lowest ($\bullet$), intermediate ($\blacktriangledown$), and highest ($\blacksquare$) RBC aggregabilities, respectively. At the highest shear rate (10 s$^{-1}$), the mean size of the aggregates was 2.4 $\pm$ 0.1 for the lowest RBC aggregability, 2.6 $\pm$ 0.1 for the intermediate level, and 3.6 $\pm$ 0.1 for the highest aggregability. Figure 8 illustrates the size distribution of the aggregates at 0.05, 0.08, 0.5, and 5 s$^{-1}$. The variance in the aggregate size increased as the shear rate was reduced. At low shear rates (0.05 and 0.08 s$^{-1}$), there were many aggregates of intermediate sizes and some very large aggregates. At 0.05 s$^{-1}$, there could be one aggregate composed of more than 300 RBCs, which represents $\frac{1}{5}$ of all RBCs in the ROI. At higher shear rates (0.5 and 5 s$^{-1}$), the size distribution of the aggregates was more uniform.

To better understand the spatial organization of the particles, the pair-correlation function $g(\mathbf{r})$ was estimated. Results at 0.05, 0.3, and 1 s$^{-1}$ are presented in Fig. 9 for the lowest and highest RBC aggregabilities. As expected, there was a greater probability that two particles be separated by
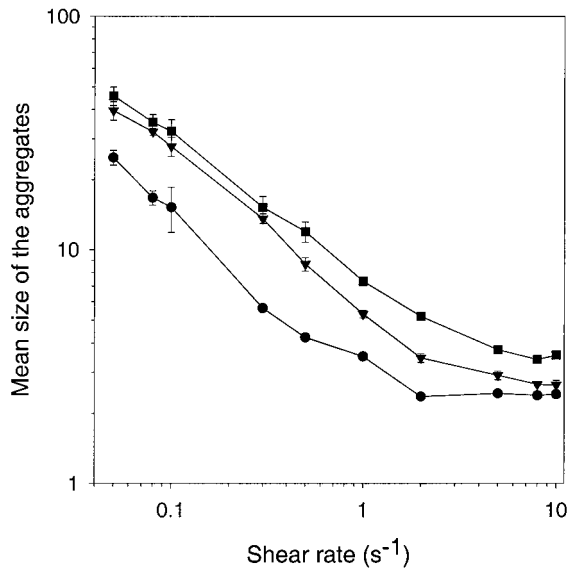
FIGURE 7   Mean size of the aggregates as a function of the shear rate, at the steady state of aggregation. Simulations of the ● lowest, ▼ intermediate, and ■ the highest RBC aggregability are presented. Results are expressed in terms of mean ± one standard deviation ($n = 4$).
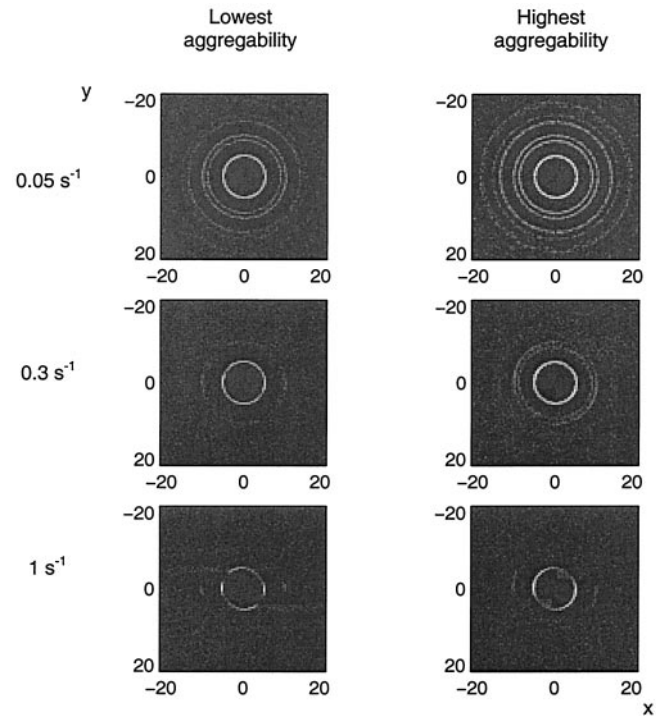


FIGURE 9   Examples of pair-correlation functions $g(\mathbf{r})$ at the lowest and highest RBC aggregabilities for shear rates of 0.05, 0.3, and 1 s$^{-1}$. Axes are expressed in micrometers.

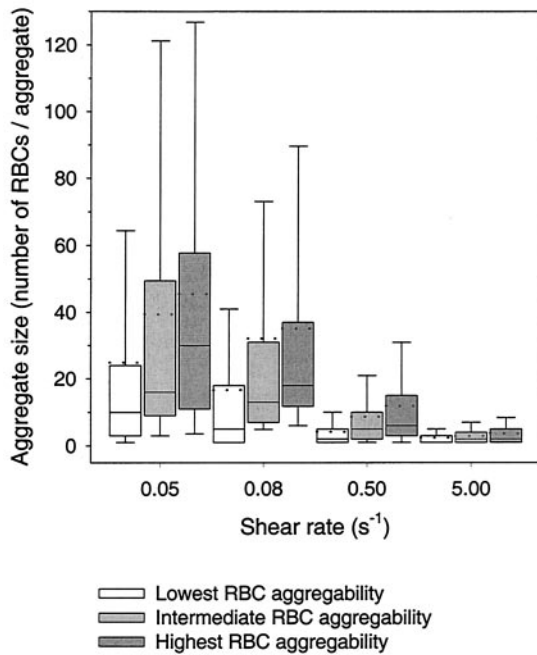5.5 $\mu$m (interior circles in each panel), which is the diameter of the RBC. An increase in the level of RBC aggregation



FIGURE 8   Size distribution of the aggregates at 0.05, 0.08, 0.5, and 5 s$^{-1}$. The boundary of the box closest to zero indicates the 25th percentile, a line within the box marks the median, and the boundary of the box farthest from zero indicates the 75th percentile. Whiskers above and below the box indicate the 90th and 10th percentile, and the dotted line indicates the mean. The □ lowest, ▨ intermediate, and ■ highest RBC aggregability are presented.

resulted in a higher probability that two RBCs be separated by multiples of the particle diameter. As the aggregation level was raised, the probability that two particles be separated by 5.5, 9.5, 11, 14.5, 16.5, and 19 $\mu$m increased (see the explanation in Discussion). In some simulations, such as 1 s$^{-1}$, the anisotropy in the spatial organization of nearby RBCs could be observed, meaning that the aggregation of the RBCs was more important along the direction of the flow ($x$). This can be observed in Fig. 10, which shows cross-sections of the pair-correlation functions along the axes $x = 0$ and $y = 0$ obtained at 0.05 s$^{-1}$ for the highest aggregability, and 1 s$^{-1}$ for the lowest aggregability. The amplitude of the function $g(\mathbf{r})$ is plotted between $-20$ and 20 $\mu$m along $x$ (for $y = 0$), and along $y$ (for $x = 0$). At 0.05 s$^{-1}$ and the highest aggregability, the probability that two particles be separated by a distance $\mathbf{r}$ is approximately the same in both directions below 20 $\mu$m. In contrast, at 1 s$^{-1}$ for the lowest aggregability, the probability that two particles be separated by their diameter is ~4 times more important along the direction of the flow ($x$) than perpendicularly ($y$).

## Ultrasound backscattering

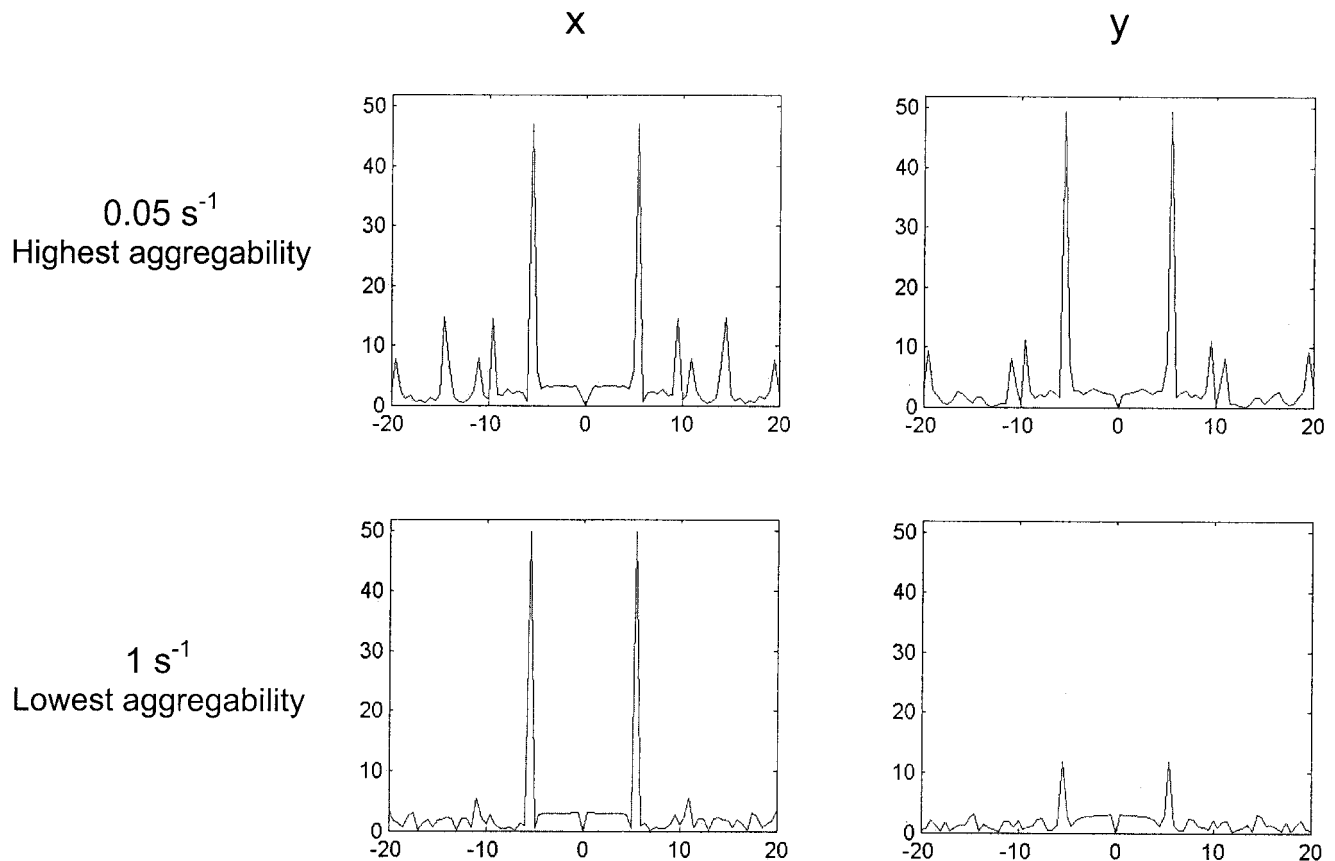The US backscattered power was computed for all simulations for a direction of insonification perpendicular to the

x

y



FIGURE 10   Cross-sections of the pair-correlation functions $g(\mathbf{r})$ along $x$ ($y = 0$) and along $y$ ($x = 0$), at 0.05 s$^{-1}$ for the highest RBC aggregability, and at 1 s$^{-1}$ for the lowest RBC aggregability. The amplitude of the pair-correlation functions is displayed between $-20$ and $20$ $\mu$m.

flow. As can be seen in Fig. 11, for a given simulation, the backscattered power increases with the iteration number, which is similar to the temporal evolution of the mean size of the aggregates (Fig. 5). As seen in Fig. 12 for any level of aggregation, the backscattered power generally decreased as the shear rate was increased, except at the highest shear rates ($>5$ s$^{-1}$), where the behavior of the backscattered power presented more variations. As expected, the backscattered power increased, in most cases, with an enhancement of the RBC aggregability, and it was maximum at 0.05 s$^{-1}$. For the lowest aggregability, the range of variation of the backscattered power was 7.6 dB between 0.05 and 10 s$^{-1}$. For the intermediate aggregability, the range was of 8.2 dB, and 11.6 dB for the highest aggregability.

In Fig. 13, the backscattered power was computed as a function of the insonification angle for the three RBC aggregabilities at 0.05 and 5 s$^{-1}$. For any given aggregability, angular variations of the order of 6 dB were observed at 0.05 s$^{-1}$. The backscattered power was maximum between approximately $-60°$ (120°) and 60° (240°), and minimum at 90° (270°). Opposing quadrants of the backscattered power appeared to be symmetrics ($\pm 180°$). At 5 s$^{-1}$, the three curves corresponding to the different aggregabilities

were not as distinct from one to another. The angular variations of the backscattered power were of the order of 5 dB for the lowest aggregability, 4 dB for the intermediate aggregability, and 3 dB for the highest aggregability. The positions of the minimum and maximum backscattered power were not as clearly defined at 5 s$^{-1}$ than at 0.05 s$^{-1}$. These results clearly indicate that the size of the aggregates is not the only determinant of the US backscattered power because, for a given size, the angle of insonification affects the intensity of the backscattered echoes.

## DISCUSSION

The simulation model of RBC aggregation mimics various configurations of RBC aggregates and computes the corresponding backscattered power. The model is innovative in that it tracks the positions of RBCs, whose motion is conditioned by the flow, and the adhesive and repulsive forces determined by the surrounding RBCs. According to the balance of forces, the aggregates could rotate with the flow or disaggregate, and thus various sizes and structures of aggregates were obtained. This behavior shown in Fig. 4
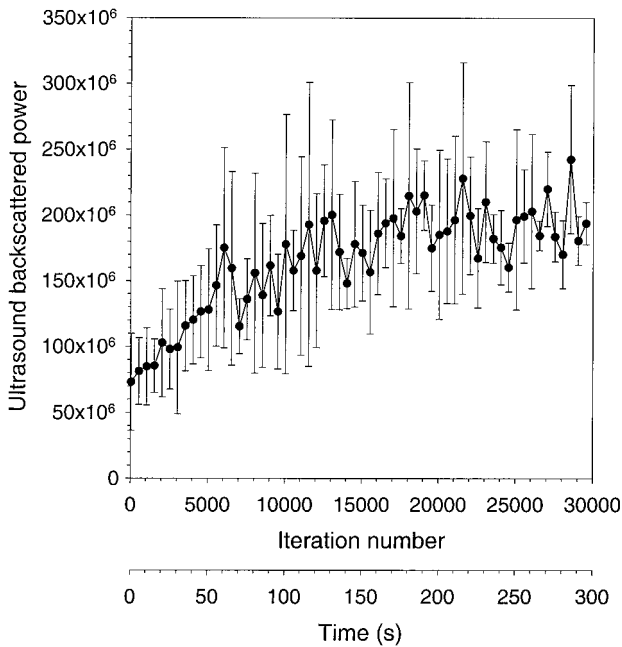
FIGURE 11 Mean backscattered power (relative units) as a function of the number of iterations (time) of the simulation model, at 0.1 s$^{-1}$, for the lowest RBC aggregability. The direction of insonification was perpendicular to the flow. Results are expressed in terms of mean $\pm$ one standard deviation ($n = 4$).



FIGURE 12 Simulated backscattered power (relative units) as a function of the shear rate for the ● lowest, ▼ intermediate, and ■ highest RBC aggregability. The direction of insonification was perpendicular to the flow. Results are expressed in terms of mean $\pm$ one standard deviation ($n = 4$).

was found to be satisfying, because it is similar to previous experimental observations, where the motion of rouleaux of human RBCs was shown under a microscope in a diluted suspension (Goldsmith and Marlow, 1972). In this last study, the RBC aggregates were found to rotate and deform, with a preferred alignment parallel to the flow.

Figure 6 demonstrated for aggregating RBCs that a wide variety of particle arrangements can be obtained at a fixed hematocrit of 40%. This resulted in a wide family of pair-correlation functions with the level of aggregation (Fig. 9), and thus of scattering behavior. The pair-correlation function illustrates the tendency of the RBCs to be aggregated and their preferred orientation. It allowed analysis of the regularity in the spatial arrangement of the RBCs, which cannot be easily observed from the realizations. From Figs. 9 and 10, it can be observed that, at 0.05 s$^{-1}$, the most probable interparticle distances were 5.5 $\mu$m (RBC diameter), 9.5, 11, and 14.5 $\mu$m. The reason for the presence of several peaks around 11 $\mu$m is illustrated in Fig. 14. For rouleau-shaped aggregates (Fig. 14, *left*), the intercellular distances are multiples of the RBC diameter, thus 5.5 and 11 $\mu$m. However, RBC aggregates can take different shapes, as illustrated in Fig. 14, *right*. In this case, the distance separating the centers of the farthest RBCs (*c* and *d*) is less than twice their diameter (9.5 $\mu$m). Other aggregate structures can be shown to result in intercellular distances of 14.5 $\mu$m.
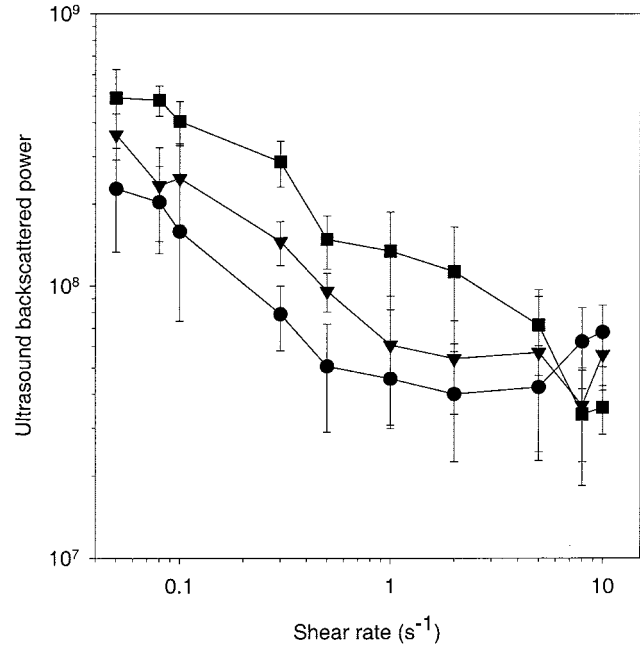
## Limitations of the packing factor, introduction of the structure factor

The properties of the structure factor are directly related to the spatial organization of the RBCs through the Fourier transformation of the function N. For nonaggregating cells, the spatial organization of the RBCs is mainly dependent on the hematocrit. Because the RBCs are much smaller than the wavelength ($f = 10$ MHz $\leftrightarrow \lambda = 157$ $\mu$m, with $c = 1570$ m/s), the backscattered power can be reasonably predicted in this case by considering only the low frequency limit of the structure factor. The structural arrangement of identical hard spheres is isotropic and the packing factor can be computed by the variance in the cell concentration of the scatterers within relatively large voxels (Mo and Cobbold, 1992). In the current modeling, aggregation of RBCs in a Couette flow resulted in an anisotropic spatial organization, which was shown to influence the backscattered signal at 10 MHz (Fig. 13). Thus, a scalar aggregation index such as the packing factor cannot fully predict the variations of the backscattered power, even at a relatively low frequency such as 10 MHz. Because RBC aggregation increases the correlation distance between the particle positions, the range of validity (in terms of frequency) of the packing factor approximation is reduced. Furthermore, there is a growing interest to characterize blood scattering at higher frequencies for high-resolution imaging. To describe the effect of red cell aggregation, it is thus preferable to refer to

FIGURE 13 Simulated backscattered power (relative units) as a function of the angle of insonification at 0.05 and 5 s$^{-1}$ for the three levels of RBC aggregability (● lowest; ○ intermediate, and ▼ highest aggregability). The angle of 0° corresponds to the alignment with the flow (x axis) going toward the US transducer, whereas 90° corresponds to measurements perpendicular to the flow (y axis).
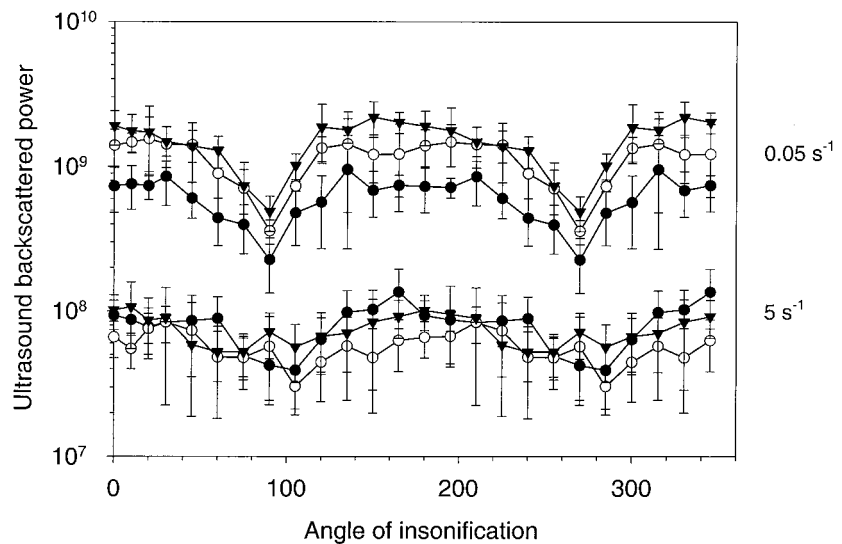
the structure factor, which describes the frequency and the orientational dependence of the backscattered power.

A 2D representation of the structure factor is presented in Fig 15. Figure 15 *a* gives the structure factor of a nonaggregated suspension of RBCs, and Fig. 15 *b* was computed from the flow-dependent simulation model of RBC aggregation at the same hematocrit (lowest aggregability, 0.05 s$^{-1}$). It was shown previously (Fontaine et al., 1999) that, even in the case of nonaggregating RBCs, the correlation in the positions of the particles resulting from their size produces oscillations in the structure factor. The same behavior is observed here in Fig. 15 *a*. The structure factors obtained from aggregating RBCs in shear flow (Fig. 15 *b*) present similar oscillations, but also anisotropic characteristics. Moreover, it can be observed that the anisotropic characteristics of the simulated structure factor vary with the range of frequencies considered. The effect of RBC aggregation on the structure factor can be more easily observed from the examples of the one-dimensional representation of S(**k**). Figure 16 illustrates cross-sections (magnitude as a function of the frequency) of the structure factor at an angle parallel to the flow (Y = 0°). The structure factor of nonaggregated RBCs at 40% hematocrit is represented in Fig. 16 *a*. The

effect of an increase in the level of RBC aggregation can be observed in Fig. 16, *b* and *c*. Increasing the aggregation (at the same hematocrit) resulted in an increase in the magnitude of the function at low frequencies (<30 MHz), and in an increase of the magnitude of the oscillations (at multiples of ~150 MHz).

## Variations of the backscattered power with the shear rate and anisotropy

Experimentally, measured variations in the ultrasonic backscattered power could be as high as 15 dB as a function of the shear rate (Yuan and Shung, 1988; Cloutier and Qin, 2000), whereas the maximum simulated variation for the highest aggregability was 11.6 dB in the current study (Fig. 12). The use of a 2D model may be the explanation for the smaller variations, because the 3D structure of the aggregates could not be considered. It is also possible that we underestimated the aggregability of porcine, equine, or human RBCs that were used in the different experimental studies reported in the literature.

Previous experimental results at 10 MHz suggested that the backscattered power could be isotropic for nonaggregated RBCs, or in the presence of large clusters, and angular-dependent for intermediate levels of aggregation (Allard et al., 1996). This was concluded from acquisitions performed in a tube between 40° and 80° using porcine whole blood (0° corresponded to the flow going toward the transducer). For the anisotropic cases, the maximum backscattered power was measured between 45° and 60°. Our simulation results did show anisotropy of the backscattered power for aggregating particles in a shear flow. The location of the maximum could not always be easily located (see Fig. 13), but, in most cases, it was found between −60° and 60° (120° and 240°). Although it is difficult to compare tube flow with Couette flow, our
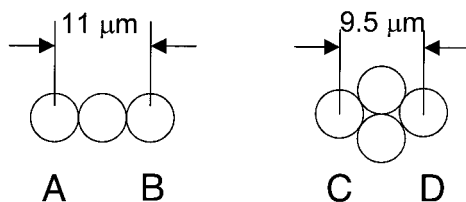


FIGURE 14 Illustration of two possible configurations of RBC aggregates. On the left, RBCs *a* and *b* are separated by twice the particle diameter, i.e., 11 μm, whereas on the right, RBCs *c* and *d* are separated by 9.5 μm.
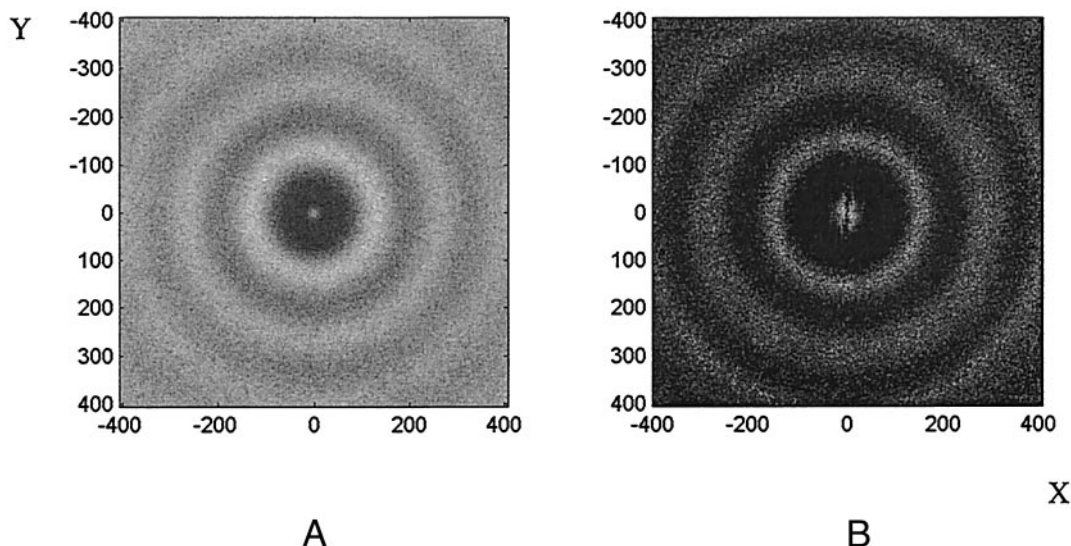
FIGURE 15 Illustrations of the structure factor $S(\mathbf{k})$ of (A) a nonaggregated suspension (hematocrit = 40%), and (B) a suspension of aggregated RBCs at 0.05 s$^{-1}$ (hematocrit = 40%, lowest aggregability). Axes are expressed in MHz.

current simulations suggest that maximum backscattering obtained in the presence of aggregated RBCs would most likely occur for a slight angulation of the transducer with respect to the flow direction. This is in agreement with the experimental observations (Allard et al., 1996).

Previous simulation results, obtained by modeling a low hematocrit of long rouleaux, suggested that the maximum backscattered power should be found perpendicular to the long axis of rouleaux (Teh and Cloutier, 2000). These results were in good agreement with experimental results obtained by using a suspension of carbon fibers (Allard et al., 1996). In this case, all scatterers were of the same size and probably oriented, on average, in the same direction. In the study of Allard et al. (1996), the maximum backscattered power was assumed to correspond to an orientation of the transducer perpendicular to the maximum section of the fiber scatterers. The spatial organization of physiological-aggregated RBCs and the corresponding acoustic response are much more complex. As the hematocrit increases, the interactions between the echoes scattered from the different aggregates are multiplied. Thus, the backscattered power cannot be predicted based on the individual backscattering cross-section of the aggregates taken separately. It is more convenient to describe the results in terms of the direction that maximizes the level of aggregation of the red cells. In the presence of a high hematocrit of aggregates, the direction of maximum backscattering is not necessarily perpendicular to the flow.

The pair-correlation functions (Figs. 9 and 10) suggest that the anisotropy in the structural arrangement of the aggregates is more important at intermediate shear rate (1 s$^{-1}$) than at very low shear rate (0.05 s$^{-1}$). However, the angular variations of the backscattered power at 10 MHz do not seem to be directly related to this observation (Fig. 13). The difficulty in explaining the behavior of the backscattered power with the angle of insonification is related to the fact that the anisotropic characteristics of the backscattered signal are frequency dependent. When a tissue is insonified with a transducer at a given central frequency and bandwidth, it is equivalent to filtering the tissue scattering properties around this frequency. It can be observed by looking at all structure factors (Fig. 15 shows some examples) that the anisotropic properties of the tissue are not constant over the whole of frequencies. We thus think that the anisotropic characteristics at a low frequency (10 MHz), observed in the current simulations, would most probably be due to anisotropy in the positioning of the particles at large distances (~30–50 $\mu$m). This is not very easy to observe from the pair-correlation function that enhances the structural properties at smaller distances (~0–15 $\mu$m).

Considering the variations of the structure factor, a slight modification of the transducer central frequency or bandwidth is likely to modify the properties of the backscattered signal. Experimental results (Foster et al., 1994; Van Der Heiden et al., 1995) and preliminary simulation results (Fontaine and Cloutier, 2000) suggested that the increase in the backscattered power with the level of aggregation is frequency dependent. Additional efforts are thus necessary to elucidate the mechanisms of US backscattering as a function of frequency and aggregation level.

## Limitations of the model

One obvious limitation of the model is the 2D ROI. A 3D modeling would allow more complex arrangements, which
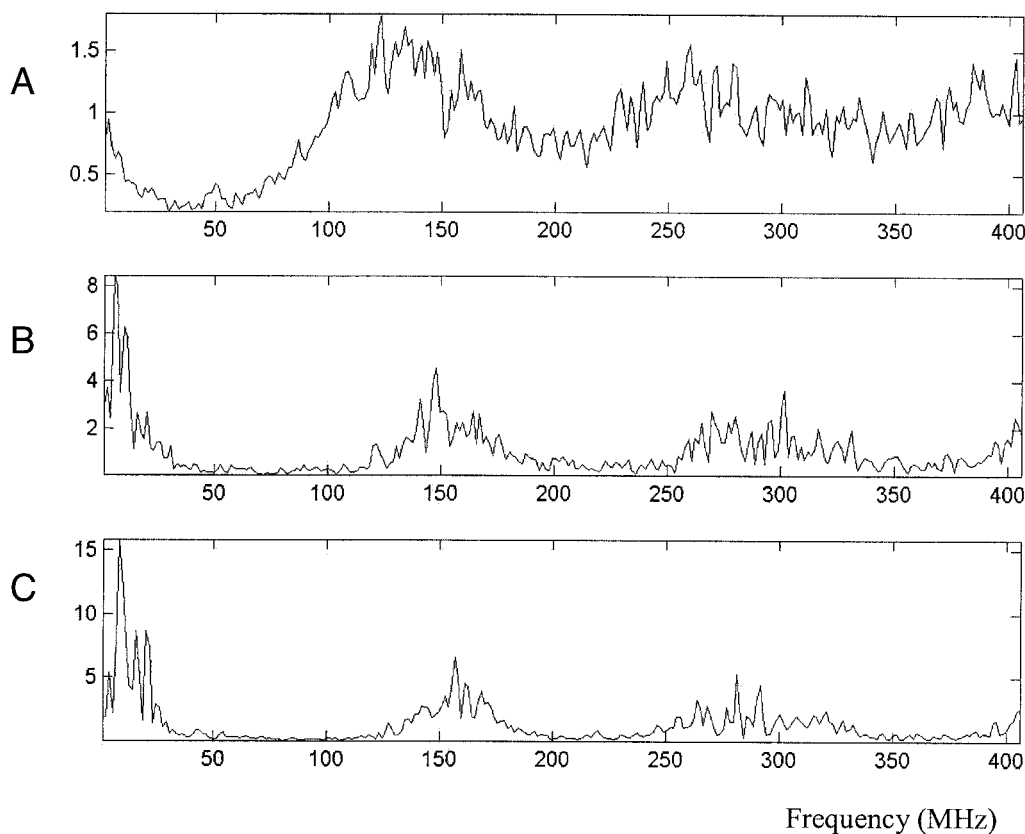
FIGURE 16 Cross-sections of the structure factors showing the amplitude as a function of the frequency (MHz) along $Y = 0$ MHz for (A) a nonaggregated suspension, (B) an intermediate level of aggregation (0.05 s$^{-1}$), and (C) a suspension with the highest level of aggregation (0.05 s$^{-1}$). All simulations were performed at 40% hematocrit.

would better mimic the physiological conditions. The 2D modeling may result in an underestimation of the size of the aggregates, and a lower backscattered power. The isotropic shape of the scatterers (RBCs were not modeled as biconcave particles) most likely diminishes the probability to form aggregates shaped as rouleaux because the adhesive force between the RBCs cannot be modulated according to their orientation. In the current model, the formation of rouleaux was indirectly enhanced by the flow, which favors a direction of aggregation parallel to it. This modeling aspect could be improved in future versions by considering the orientation of the cells. Also, at the highest shear rates, the displacement of the particles resulting from the application of the flow during one time interval became quite important. This displacement in a single iteration might be too large in comparison to the small-scale phenomenon of RBC aggregation, and particle superposition could more likely occur. This may be the explanation for the lack of consistency of the backscattered power, seen in Fig. 12, at the highest simulated shear rates ($>5$ s$^{-1}$). Although the variance in the mean size of the aggregates was small (Fig. 7), variability in the level of particle superposition modified the spatial arrangement of RBCs, and consequently the backscattered power.

One can argue that the dynamic model of aggregation is a simplistic approximation of the real biophysical interactions involved among RBCs, and that the choice of the displacements attributed to the different forces was somewhat subjective. The quantitative values of the adhesive and repulsive forces are not known from the literature, and they may be influenced by a number of factors such as the type and concentration of macromolecular proteins, the membrane properties of RBCs, the temperature, the pH, and they can vary significantly among individuals. The present model modulated the degree of aggregation by varying the capture radius for the interaction and displacements attributed to the adhesive forces. Although of hypothetical value, this modeling approach may reflect the variation of aggregation due to the type, size, and configuration of the plasmatic macromolecules involved (fibrinogen, immunoglobulins, haptoglobin, ceruloplasmin, C-reactive protein, $\alpha_2$-macroglobulin, and possibly others) (Weng et al., 1996). Although this model may be criticized, it was shown to be powerful to study the effect of various geometrical configurations of aggregated RBCs on the US scattered signal. It is believed that the hypotheses of the model are acceptable to pursue this goal. The results shown in the previous section demonstrate that the proposed simulation model is

an efficient method to model various configurations of RBC aggregates and to study their effect on the US backscattered signal. Furthermore, as mentioned before, the kinetics of aggregation (Figs. 5 and 11) are in good agreement with experimental observations.

## CONCLUSION

US backscattering by blood is a complex phenomenon, affected by the level of RBC aggregation, the hematocrit, the US beam characteristics, and the angle of insonification. The simulation model presented in the current study is an efficient tool to predict the ultrasonic response to various RBC spatial organizations. The motion of interacting particles in shear flow was modeled, and it was shown to be similar to that of aggregating RBCs. The results demonstrated that variations in the ultrasonic backscattered power can be explained by considering the properties of the microstructure of the RBCs. We showed that the polydispersity in the size of the aggregates, the correlation in the positions of the RBCs, the shape, and orientation of the scatterers must be considered to establish a suitable index of aggregation measurable by US. Although limited to two dimensions, this model can contribute to the better understanding of the effect of the size and shape of RBC aggregates on the backscattering properties. Additional experimental results would be required to validate the simulations as a function of the angle of insonification. It would also be interesting to study the backscattering properties at various frequencies, hematocrits, and under different flow conditions.

## REFERENCES

Allard, L., G. Cloutier, and L. G. Durand. 1996. Effect of the insonification angle on the Doppler backscattered power under red blood cell aggregation conditions. *IEEE Trans. Ultrason. Ferroelect. Freq. Contr.* 43: 211–219.

Armstrong, J. K., H. J. Meiselman, and T. C. Fisher. 1999. Evidence against macromolecular "bridging" as the mechanism of red blood cell aggregation induced by nonionic polymers. *Biorheology.* 36:433–437.

Bäumler, H., E. Donath, A. Krabi, W. Knippel, A. Budde, and H. Kiesewetter. 1996. Electrophoresis of human red blood cells and platelets. Evidence for depletion of dextran. *Biorheology.* 35:333–351.

Bäumler, H., E. Donath, L. Pratsch, and D. Lerche. 1989. Aggregation and disaggregation of human red blood cells in neutral polymer electrolyte solutions. *In* Hémorhéologie et Agrégation érythrocytaire. Théorie et Application cliniques. J. F. Stoltz, M. Donner, and A. L. Copley, editors. Éditions Médicales Internationales, Paris. 24–37.

Berger, N. E., R. J. Lucas, and V. Twersky. 1991. Polydisperse scattering theory and comparisons with data for red blood cells. *J. Acoust. Soc. Am.* 89:1394–1401.

Brooks, D. E., G. Russell, G. Janzen, and J. Janzen. 1980. Mechanisms of erythrocyte aggregation. *In* Erythrocyte Mechanics and Blood Flow. G. R. Cokelet, H. J. Meiselman, and D. E. Brooks, editors. Liss, A. R., Inc., New York. 119–140.

Chabanel, A., M. H. Horellou, J. Conard, and M. M. Samama. 1994. Red blood cell aggregability in patients with a history of leg vein thrombosis: influence of post-thrombotic treatment. *Br. J. Haematol.* 88:174–179.

Chien, S. 1975. Biophysical behavior of red cells in suspensions. *In* The Red Blood Cell. D. M. Surgenor, editor. Academic Press, New York, San Francisco, London. 1031–1133.

Chien, S. 1976. Electrochemical interactions between erythrocyte surfaces. *Thromb. Res.* 8:189–202.

Chien, S. 1981. Electrochemical interactions and energy balance in red blood cell aggregation. *In* Topics in Bioelectochemistry and Bioenergetics. John Wiley & Sons, Chichester, New York, Brisbane, Toronto. 73–112.

Cloutier, G., and Z. Qin. 1997. Ultrasound backscattering from non-aggregating and aggregating erythrocytes—a review. *Biorheology.* 34: 443–470.

Cloutier, G., and Z. Qin. 2000. Shear rate dependence of ultrasound backscattering from blood samples characterized by different levels of erythrocyte aggregation. *Ann. Biomed. Eng.* 28:399–407.

Copley, A. L., R. G. King, and C. R. Huang. 1976. Erythrocyte sedimentation of human blood at varying shear rates. *In* Microcirculation. J. Grayson and W. Zingg, editors. Plenum Press, New York. 133–134.

Donath, E., and A. Voigt. 1986. Electrophoretic mobility of human erythrocytes. On the applicability of the charged layer model. *Biophys. J.* 49:493–499.

Fontaine, I., M. Bertrand, and G. Cloutier. 1999. A system-based approach to modeling the ultrasound signal backscattered by red blood cells. *Biophys. J.* 77:2387–2399.

Fontaine, I., and G. Cloutier. 2000. Frequency dependence of simulated ultrasound signals backscattered by aggregating red blood cells. *In* Acoustical Imaging. M. Halliwell and P. N. T. Wells, editors. Kluwer Academic/Plenum Publishers, New York, Boston, Dordrecht, London, Moscow. 297–302.

Foster, F. S., H. Obara, T. Bloomfield, L. K. Ryan, and G. R. Lockwood. 1994. Ultrasound backscatter from blood in the 30 to 70 MHz frequency range. *IEEE Ultrason. Symp. Proc.* 1599–1602.

Goldsmith, H. L. and J. Marlow. 1972. Flow behaviour of erythrocytes. I. Rotation and deformation in dilute suspensions. *Proc. Royal Soc.* 182: 351–384.

Jan, K. M., and S. Chien. 1972. Role of the electrostatic repulsive force in red cell interactions. 7th European Conference Microcirculation. 11: 281–288.

Jan, K. M., and S. Chien. 1973. Role of surface electric charge in red blood cell interactions. *J. Gen. Physiol.* 61:638–654.

Landini, L., and L. Verrazzani. 1990. Spectral characterization of tissues microstructure by ultrasounds: a stochastic approach. *IEEE Trans. Ultrason. Ferroelect. Freq. Contr.* 37:448–456.

Lim, B., P. A. J. Bascom, and R. S. C. Cobbold. 1996. Particle and voxel approaches for simulating ultrasound backscattering from tissue. *Ultrasound Med. Biol.* 22:1237–1247.

Lucas, R. J., and V. Twersky. 1987. Inversion of ultrasonic scattering data for red blood cell suspensions under different flow conditions. *J. Acoust. Soc. Am.* 82:794–799.

Mo, L. Y. L., and R. S. C. Cobbold. 1992. A unified approach to modeling the backscattered Doppler ultrasound from blood. *IEEE Trans. Biomed. Eng.* 39:450–461.

Neumann, F. J., H. A. Katus, E. Hoberg, P. Roebruck, M. Braun, H. M. Haupt, H. Tillmanns, and W. Kübler. 1991. Increased plasma viscosity and erythrocyte aggregation: indicators of an unfavourable clinical outcome in patients with unstable angina pectoris. *Br. Heart J.* 66:425–430.

Razavian, S. M., V. Atger, P. H. Giral, M. Cambillau, M. Del-Pino, A. C. Simon, N. Moatti, and J. Levenson. 1994. Influence of HDL subfractions

on erythrocyte aggregation in hypercholesterolemic men. *Arterioscler. Thromb.* 14:361–366.

Razavian, S. M., M. Del Pino, A. Simon, and J. Levenson. 1992. Increase in erythrocyte disaggregation shear stress in hypertension. *Hypertension.* 20:247–252.

Schmid-Schönbein, H., and E. Volger. 1976. Red-cell aggregation and red-cell deformability in diabetes. *Diabetes.* 25:897–902.

Shehada, R. E. N., R. S. C. Cobbold, and L. Y. L. Mo. 1994. Aggregation effects in whole blood: influence of time and shear rate measured using ultrasound. *Biorheology.* 31:115–135.

Shung, K. K., and G. A. Thieme. 1993. Ultrasonic Scattering in Biological Tissues. CRC Press, Boca Raton, Ann Arbor, London, Tokyo.

Sigel, B., J. Machi, J. C. Beitler, J. R. Justin, and J. C. U. Coelho. 1982. Variable ultrasound echogenicity in flowing blood. *Science.* 218: 1321–1323.

Teh, B. G., and G. Cloutier. 2000. The modeling and analysis of ultrasound backscattering by red blood cell aggregates with a system-based approach. *IEEE Trans. Ultrason. Ferroelect. Freq. Contr.* 47:1025–1035.

Twersky, V. 1975. Transparency of pair-correlated, random distributions of small scatterers, with application to the cornea. *J. Opt. Soc. Am.* 65:524–530.

Twersky, V. 1987. Low-frequency scattering by correlated distributions of randomly oriented particles. *J. Acoust. Soc. Am.* 81:1609–1618.

Ursea, R., J. Coleman, R. H. Silverman, F. L. Lizzi, S. M. Daly, and W. Harrison. 1998. Correlation of high-frequency ultrasound backscatter with tumor microstructure in iris melanoma. *Ophthalmology.* 105: 906–912.

Van Der Heiden, M. S., M. G. M. De Kroon, N. Bom, and C. Borst. 1995. Ultrasound backscatter at 30 MHz from human blood: influence of rouleau size affected by blood modification and shear rate. *Ultrasound Med. Biol.* 21:817–826.

Varghese, T., and K. D. Donohue. 1993. Characterization of tissue microstructure scatterer distribution with spectral correlation. *Ultrasonic Imaging.* 15:238–254.

Weng, X., G. Cloutier, R. Beaulieu, G. O. Roederer. 1996. Influence of acute-phase proteins on erythrocyte aggregation. *Am. J. Physiol. Heart Circ. Physiol.* 40:H2346–H2352.

Yuan, Y. W., and K. K. Shung. 1988. Ultrasonic backscatter from flowing whole blood. I: Dependence on shear rate and hematocrit. *J. Acoust. Soc. Am.* 84:52–58.

Zhang, J., J. L. Rose, and K. K. Shung. 1994. A computer model for simulating ultrasonic scattering in biological tissues with high scatterer concentration. *Ultrasound Med. Biol.* 20:903–913.